RESEARCH ARTICLE | FEBRUARY 18 2020

Transverse localization of light in laser written designed disorder

A. Gianfrate ; L. Dominici ; D. Ballarini ; D. Sanvitto ; M. Leonetti

Appl. Phys. Lett. 116, 071101 (2020)
https://doi.org/10.1063/1.5142161

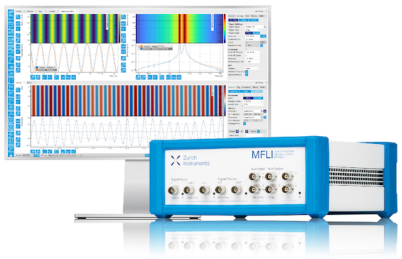

Applied Physics Letters ARTICLE scitation.org/journal/apl

Transverse localization of light in laser written designed disorder

Cite as: Appl. Phys. Lett. **116**, 071101 (2020); doi: 10.1063/1.5142161
Submitted: 10 December 2019 · Accepted: 2 February 2020 ·
Published Online: 18 February 2020

A. Gianfrate,[a),b)] L. Dominici, D. Ballarini, D. Sanvitto,[c)] and M. Leonetti[d)]

AFFILIATIONS

CNR NANOTEC, Istituto di Nanotecnologia, via Monteroni, I-73100 Lecce, Italy

[a)]**Electronic mail:** antonio.gianfrate@nanotec.cnr.it
[b)]**Also at:** Dipartimento di Matematica e Fisica, Universitá del Salento, Via Arnesano, I-73100 Lecce, Italy.
[c)]**Also at:** INFN, Istituto Nazionale di Fisica Nucleare, Sezione di Lecce, I-73100 Lecce, Italy
[d)]**Also at:** Center for Life Nano Science @ Sapienza, Istituto Italiano di Tecnologia, Viale Regina Elena, 291, I-00161 Roma, Italy.

ABSTRACT

Transverse Anderson localization provides the lateral confinement of electromagnetic waves in disordered systems that are invariant along the propagation direction. Here, we demonstrate a disorder induced confinement in glass microstructures where disorder is fabricated *ad hoc* by the femtosecond direct laser writing technique. By employing a high numerical aperture objective, we are able to write parallel arrays of tiny tubes with a refractive index higher than the surrounding glass and to arrange them in a disordered fashion in the transversal plane. We demonstrate that these paraxial scatterers are supporting transverse localization and that the confinement strength depends on the disorder properties. The proposed approach, which relies on a user-controlled positioning of individual scatterers, allows us to finely tune the structural design, maximizing the transversal confinement.

Anderson localization[1] is among the most counterintuitive transport phenomena observed in disordered systems. It is a disorder-induced phase transition in the wave behavior that drives the standard diffusion to a localized regime in which the material behaves as an insulator, and has been demonstrated for a variety of systems.[2–4] For three dimensional light waves, localization is still an open challenge characterized by debated experimental results.[5–7] In the framework of disordered photonics, localization is usually studied resorting to randomly distributed scatterers such as microparticles embedded in a solid matrix or dispersed in a liquid suspension. With these approaches, the position of the individual scatterer is uncontrolled, and thus, the particular disorder configuration may not be defined at the fabrication stage. On the other hand, it is possible to control the average properties of the composite material, such as the transport mean free path and optical thickness.[8]

A rising trend, however, is the one of the "designed disorders"[9,10] in which a complex system, composed of apparently random structures, is instead fabricated by scatterers arranged in pre-defined patterns designed to improve the confinement performances. These peculiar configurations allow the realization of Anderson localizing media with the arbitrary structure factor and user-defined photonic bandgap.

While it is very difficult to manipulate three dimensional disordered materials, it is possible to control the scatterer positions in systems with lower dimensionality. Indeed, the transverse Anderson localization (TAL) is a phenomenon typical of a two-dimensional disordered structure where it is possible to control the arrangement of the disorder. TAL[11] is achievable in systems invariant along the propagation direction and disordered in the transverse plane, e.g., a set of randomly arranged but strictly parallel tubes. In their seminal paper,[12] Schwartz and co-workers exploited a photorefractive crystal to generate longitudinally invariant and reconfigurable scattering patterns composed of tubes aligned along the direction of propagation (the "paraxial scatterers," or PSs). Transverse localization is particularly appealing for optical transmission because it may be employed for the fabrication of optical fibers based on disorder (Disordered Optical Fibers, DOF),[13,14] which are promising devices in several fields including imaging,[15] lasing,[16] nonlinear optics,[17,18] and quantum key distribution.[19]

In this work, we demonstrate the realization of DOF based on the direct laser writing of PSs enabling us to export the advantage of the designed disorder to optical fibers. We use a femtosecond direct laser writing (FDLW) technique commonly employed for the fabrication of waveguides with complex shapes in the visible range.[20,21]

FDLW is based on two photon nonlinear absorption of highly compressed pulses (with energy in the range of μJ) producing an optical breakdown process due to the ionization of a large number of electrons that, in turn, transfer energy to the lattice. As a result of the irradiation, the material undergoes a phase or structural modification, leaving behind a localized permanent increment of the refractive index. By moving at constant speed the sample under the laser shine, it is possible to write a homogeneous tube with a refractive index different from the surrounding materials and able to support a single electromagnetic mode. This technique allows us to fabricate single mode waveguides that can be arranged in a complex fashion, in order to implement interferometers or other sophisticated optical elements.[22]

Here, we are interested in a different form of confinement: our aim is to produce PSs, acting as an array of scatterers able to sustain transverse localization. Thus, in a DOF, light does not propagate in a single tube, but instead it is confined by a multiple scattering process involving the interference between several PSs. By using a 0.65 NA objective to write small (two μm sized) structures, we are able to avoid waveguiding inside single and large (typically ten micrometer in diameter) tubes, which are instead obtained upon laser writing with smaller NA objectives.[22–24] By means of this technique, we can explore the behavior of the TAL localization not only varying the structural disorder strength but also with respect to the main design and fabrication parameters: the lattice parameter, the defect size, and the Δn refractive index change. However, the two latter parameters are subject to more severe limitations, being related to the physics of the writing mechanism.

The writing setup is powered by a 10 kHz repetition rate, 30 fs pulse laser with a central wavelength of 800 nm, able to reach up to 20 GW peak power. The pulse chirping is minimized by the use of specific chirped mirrors and reflective objective. The substrate used to fabricate the DOF structure is a bulk silica glass. We used standard commercially available Menzel-Glaser 75 mm × 25 mm × 1 mm microscope slides. Typical writing conditions are set to an input power of 15 mW and a translation speed of 1.25 mm/s along the writing direction, tuned in order to avoid the prolonged exposition of the same spatial region. The long working distance (1.9 mm) of the reflective objective allows us to access all the depth of our 1 mm thick sample and in particular to comfortably scan the writing depth of the current DOFs. A set of six PSs, written close to the surface, are shown in Fig. 1(b).

The refractive index mismatch obtained by using our writing technique is retrieved on a transmission interferometric setup,[25] shown in Fig. 1(a), using a 735 nm cw laser. The digital off-axis holography technique allows us to obtain a spatial map of the phase delay in the parallel section of the scatterer. An example of the obtained interference patterns is shown in the inset of Fig. 1(a). The computational Fast Fourier transform routines allows us to access the modulational data directly in the reciprocal space and plot the phase information back into real space. The result is shown in Fig. 1(c). The two slightly brighter vertical stripes represent our laser written PSs. A cross profile of the phase (along the red line) is highlighted in Fig. 1(d), where the dots are the experimental values and the solid red line is a Gaussian fit. Indeed, the single PS results to be 1.46 μm FWHM wide, with a maximum phase retard of 0.66 rad, between the unmodified boundary glass and the scatterer center. This value represents the integrated phase

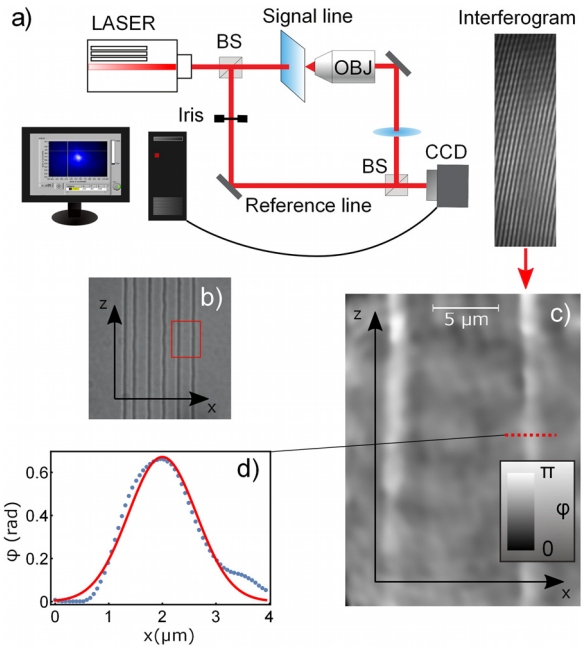

FIG. 1. Digital holography setup and scatterer characterization. (a) Sketch of the off-axis digital holography setup. The technique exploits the interference between a signal line and a reference line. The resulting typical interferogram is represented in the upper right inset. (b) Phase contrast microscopy image of six parallel written PSs. (c) Off-axis digital holography map of the phase delay induced by two scatterers. (d) Phase profile (dots) and Gaussian fit (solid red line) along a section of a scatterer.

delay along the central vertical diameter of the PS. The associated mean index variation is estimated to be $\Delta n \approx (1.25 \pm 0.5) \cdot 10^{-2}$ in the very center. Both the size and Δn of the written PSs are close to the limit values, which can be reached on our setup, as evaluated upon the application of the Rayleigh criterion or the comparison with values from the literature.[23,26] Apart from the use of a higher NA (e.g., immersion) objective, also a combination of laser writing and chemical etching could potentially extend the range of the accessible index variation and size parameters, even below the diffraction limit, as demonstrated in a recent state of the art work.[27–29]

The transverse confinement is sustained by a disordered pattern of PSs, which is invariant along the propagation axis of the fiber. This structure is realized in our glass DOF by a square array of 2304 individual PS, arranged in a randomized lattice location over a 240 μm × 240 μm square section. To realize the structure, we need to design the transverse coordinates of the scatterers, which are then passed to our software that automatically sets the motor positions in order to write at each coordinate a single PS. Every scatterer is a tube with an approximate diameter of two micrometers, all running in the same direction for a longitudinal length between 5 and 30 mm, depending on the specific sample. We start from the coordinates of a square lattice with side δ and added to each point m a random displacement $[\Delta x_m, \Delta y_m] = [\delta\chi\theta_x(m), \delta\chi\theta_y(m)]$, where $\theta_x(m)$ and $\theta_y(m)$ are uniformly distributed random numbers in the interval $(-0.5, 0.5)$ and χ is a user defined parameter defining the average disorder strength

(displacement with respect to the lattice locations) and is set between 0 and 1, see Figs. 2(a)–2(c). Taking into account that the diameter of the single scatterer is ≈2 μm, we fabricated DOF with a lattice parameter $\delta > 5\,\mu$m in order to minimize overlapping tubes, which would produce uncontrolled optical structures. When χ is close to 0, a negligible random displacement is added to the coordinates, and thus, the writing session produces a square lattice structure. This 2D photonic crystal structure is however unable to guide light due to the poor refractive index mismatch.[30] When χ is close to 1, the displacement is on the order of the lattice parameter δ itself, thus producing a completely disordered pattern of parallel tubes.

The advantage of the proposed approach with respect to previous strategies[13,14] is that it allows the direct placement of any individual scatterer, thus enabling to finely tune the disorder properties in order to optimize the confinement strength. To measure the confinement capability of our fibers as a function of the structural parameters, we exploited an experimental setup similar to the one employed by the authors in Ref. 31 in which the DOF output is measured with a camera. In our protocol, coherent light from a probe beam (source: Oxxious LBX-638 nm, maximum power 200 mW, see Fig. 2) is coupled onto the disordered fiber. In order to easily translate the position of the input beam, we used a pinhole (200 μm diameter) mounted on two motorized actuators. An image of the pinhole is then produced with a de-magnifying telescope (factor 10) on the input facet of the fiber, producing a 20 μm spot at the input whose position may be set by controlling the pinhole position. Two computer controlled actuators enable the automatic scan of the fiber input facet. For each input position, we obtain the correspondent output: in general, the position of maximum intensity in the output plane is conformally located with respect to the transverse input coordinate. The typical output images from DOFs realized with different fabrication parameters are shown in Figs. 2(d)–2(i). We clearly observe that the maximum confinement is retrieved for $\chi = 0.6$. As a comparison, we also report in Fig. 2(i) the intensity profile retrieved for propagation in a bare glass, i.e., in a sample without PS inscribed. To estimate the strength of the lateral confinement, we study the intensity profile at the output plane as a function of a radial coordinate, i.e., the distance from the transverse position of the input at the entrance facet.

A key feature of the Anderson localization is the averaging over the disorder configurations. The DOFs we fabricate are characterized by a fixed configuration of the disorder, and thus, in order to probe different realizations, we changed the input location of the probe beam by translating the position of the pinhole. In a standard measurement protocol, we took the output patterns relative to 100 input locations (regularly positioned in a raster scan fashion along the whole input square array) and retrieve a decay length ξ_C for each one. As demonstrated in Ref. 32, the "average-over-input" is comparable to an "average-over-disorder" operation, and thus, we exploited the former to demonstrate the presence of transverse localization.

In Fig. 3, we report the intensity profile as a function of $\rho = \sqrt{x^2 + y^2}$, which represents the transverse distance from the input location [x and y are indicated in Fig. 2(f)]. The plot has been obtained by averaging 100 output configurations, after aligning the output images. To do this, the images have been translated in order for

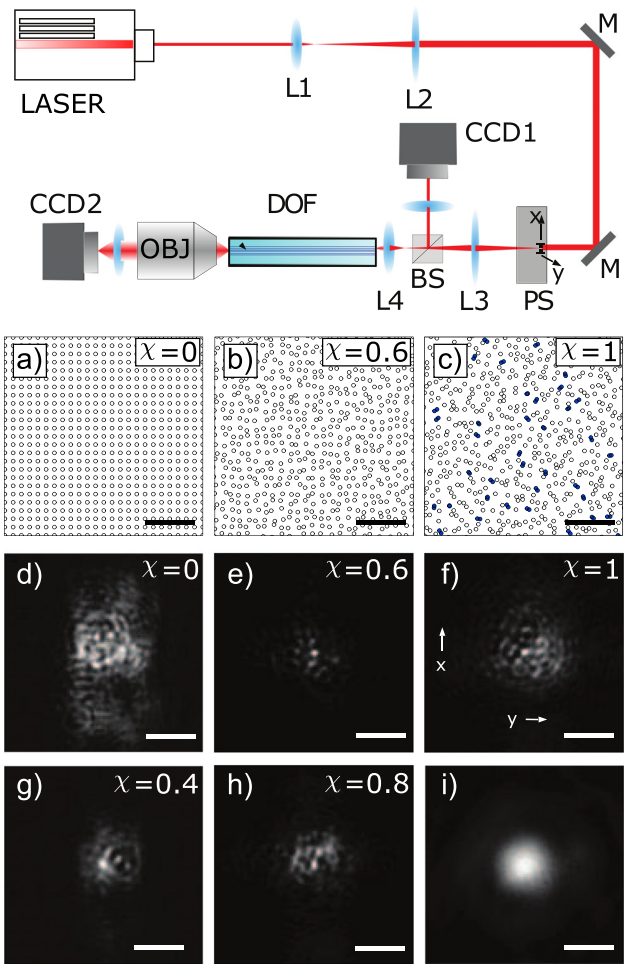

FIG. 2. The scheme depicts the experimental setup. L1, L2 and L3, L4 are lenses working as magnifier and de-magnifier telescopes. M: mirror, CCD1 and CCD2: cameras, PS: actuator mounting the pinhole, OBJ: collection objective, and BS: beam splitter. Panels (a)–(c) show the model distribution of transverse scatterers for different values of the disorder degree χ, and the merging scatterers are highlighted in blue. Panels (d)–(i) show the images of a typical transmitted intensity pattern varying χ. The pattern in panel (i) is obtained from a homogeneous (without laser written scatterers) glass support. The lateral size of the entire DOF is 240 μm × 240 μm. The scale bar is 30 μm.

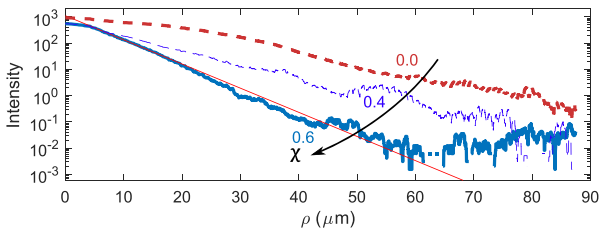

FIG. 3. Transverse localization with different degrees of disorder. Solid blue line: radial mean profile (intensity as a function of the radial coordinate $(\rho = \sqrt{x^2 + y^2})$), obtained by averaging 100 output images relative to that many input configurations, in the case of $\chi = 0.6$. The fit with an exponential function (localization length $\xi_C = 4.7\,\mu$m) is reported as a thin red line. As a comparison, we also show the experimentally retrieved profile obtained with $\chi = 0.4$ (blue thin dashed) and $\chi = 0$ (red thick dashed).

their origin to be centered with the relative input location. Then, the mean radial intensity profile has been obtained upon a further averaging along the azimuth. The profile reported in a logarithmic scale clearly demonstrates an exponentially decaying behavior observed along 5 decades. This is a strong signature of Anderson localization.[12,13] The blue solid line is obtained for $\chi = 0.6$ and $\delta = 5\,\mu$m. The data are then fitted with an exponential function (red solid line): $A\exp(-\rho/\xi_C)$, where A is a normalization parameter and ξ_C is the localization length, equal to 4.7 μm for the data of Fig. 3. As a comparison, we report also the result for measurements obtained for the structure with the same transverse density of scatterers but with different degrees of disorder ($\chi = 0.4$ for the blue thin dashed line and $\chi = 0.0$ for the red dashed line). A twofold-threefold larger spatial extension of the output profile and a deviation from the single exponential behavior are evident.

We further characterized the behavior of ξ (obtained by averaging ξ_C on several samples) as a function of the lattice size δ, at a fixed disorder degree ($\chi = 0.5$). In Fig. 4(a), we show that ξ decreases by decreasing the lattice parameter δ, and thus, the configuration of maximum confinement is here obtained for $\delta = 5\,\mu$m. Our approach can be potentially extended also to study the impact of larger or smaller PS size. In the latter case, one has to deal with higher NA objectives and to work very close to the threshold writing power. This would result in sub-micrometric defects, which are however characterized by a very small (10^{-4}) Δn, thus possibly compromising the onset of localization at all. On the other hand, a completely different approach such as the use of a combination of laser irradiation and chemical etching,[29] could provide instead very large Δn (up to 0.5/0.8, depending on the substrate material), nonetheless ensuring a submicrometer defect size.

As anticipated, the TAL is a fundamental mechanism, which is dependent on the degree of disorder. Hence, we show in Fig. 4(b) the measured ξ as a function of the disorder strength χ at fixed $\delta = 5\,\mu$m. While the radial extension is large (poor confinement strength) in the total absence of disorder ($\chi = 0$), a small amount of disorder already triggers for a stronger confinement.[33] By further increasing χ, the localization strength shrinks up to $\chi = 0.6$. Increasing χ above 0.6 produces instead an enlargement of the output distribution with respect to its minimum value, which is also visible in panels of Figs. 2(f) and 2(h). This inversion is due to a small amount of merging PS (an effect appearing for $\chi > 0.6$, due to the scatterer size of 2.0 μm), which is working as a single one, thus effectively decreasing the overall scattering strength [please note the blue highlighted merging scatterers for $\chi = 1$ in Fig. 2(c)]. We estimate that 5% of the scatterers are overlapping at $\chi = 0.8$, while more than 15% are overlapping with $\chi = 1$.

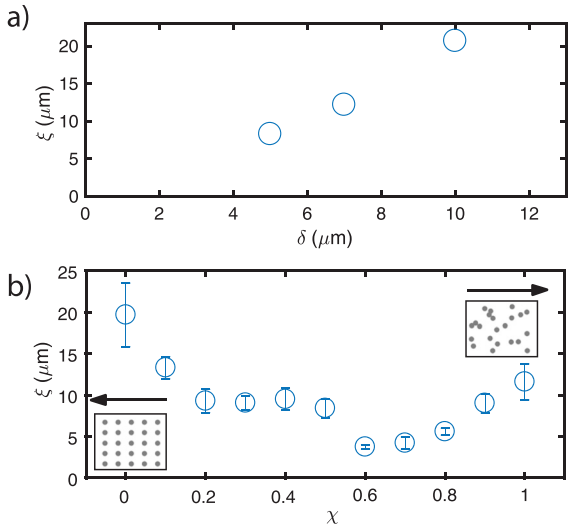

FIG. 4. (a) Localization length ξ as a function of the lattice scale parameter δ, for a fixed degree of disorder ($\chi = 0.5$). Error bars are smaller than the markers. (b) Localization length ξ vs the disorder degree parameter χ, for a fixed scale size ($\delta = 5\,\mu$m).

The onset of localization in three dimensions is predicted by the Ioffe–Regel criterion stating that the product of the wavevector (K) and the transport mean free path (ℓ^*) should be smaller than one: $K\ell^* < 1$. In the case of the two dimensional TAL, the transverse quantities are instead the relevant ones.[12] To estimate the transverse wavevector K_t, we notice that in our experiments, light can be coupled efficiently only within an input angle of $\Theta = 12$ mrad. The maximum transverse wavevector is thus[34] $K_t = K \cdot \sin\Theta = 2\pi/\lambda \cdot \sin\Theta = 0.12\,\mu\text{m}^{-1}$. This value of K_t is consistent with the onset of localization if the transport mean free path in our fibers is smaller than the associate transverse wavelength, i.e., $\ell^* < 8.4\,\mu$m. An estimate of the mean free path (ℓ) can be given resorting to the formula:[35] $\xi = \ell e^{\pi K_t \frac{\ell}{2}}$, which provides $\ell = 3\,\mu$m.

We also estimated the propagation losses, upon performing experiments on DOF with different lengths, retrieving an attenuation of 3 dB/cm. This limited efficiency, an important parameter from an application point of view, is mainly due here to the low index contrast. It could be potentially improved by enhancing the longitudinal homogeneity, by using high repetition rate writing lasers, or by increasing the refractive index mismatch, e.g., applying the etching of the written PS.[27–29] An increase in Δn has the effect to reduce the localization length and also increases scattering losses from incidental defects. Thus, the overall effect would be strongly dependent on the quality itself of the PSs along the written DOF line, but in principle not only the localization length but also the loss can be optimized upon a larger Δn. The best performance device would be realized by exporting the technique to standard silica fibers, thus adding disorder induced localization to standard step index confinement.

From an application point of view, the cost for the fabrication of the DOFs would be mainly ascribed to the power supply of the femtosecond laser, which is increased by the very long duration of the sequential writing of a large number of PSs. In order to overcome such a limitation, the writing technique would strongly benefit in future applications from parallelization, e.g., by employing a holographic technique[36] to write several PSs at a single pass, upon which one could dramatically reduce the fabrication time.

In summary, we present here a fabrication scheme that enables us to build microstructures supporting confinement induced by disorder thanks to transverse Anderson localization. The proposed approach, based on the individual fabrication of paraxial scatterers, enables the designer to control the scattering properties of the medium, thus exporting the concepts of the designed disorder to the field of optical fibers. We exploited this flexibility in order to properly optimize the disorder parameters: indeed, we optimized both the average scatterer distance and the strength of the disorder. With our approach, the localization phenomena could be studied against

different disordered lattices, hexagonal vs squared, or a kind of randomness (e.g., Gaussian instead of flat distributions of off-axis lattice sites), rather than simply vs the random degree strength. The direct laser writing of PS thus has the potential to enable the fabrication and study of DOF based on more sophisticated confinement mechanisms such as bandgap formation mediated by hyperuniformity or topological insulation. Furthermore, the glass could be an active or nonlinear medium,[12,15,17] thus opening a number of doors to even more variegated effects for both applications and scientific explorations.

M.L. and A.G. thank "Fondazione CON IL SUD," Grant "Brains2south," Project "Localitis." A.G., L.D., D.B., and D.S. thank the ERC project ElecOpteR (No. 780757). We acknowledge also the project FISR - C.N.R. "Tecnopolo di nanotecnologia e fotonica per la medicina di precisione" - CUP B83B17000010001 and "Progetto Tecnopolo per la Medicina di precisione, Deliberazione della Giunta Regionale n. 2117 del 21/11/2018."

REFERENCES

[1]P. W. Anderson, Phys. Rev. **109**, 1492 (1958).
[2]E. Abrahams, *50 Years of Anderson Localization* (World Scientific, 2010).
[3]H. Hu, A. Strybulevych, J. Page, S. E. Skipetrov, and B. A. van Tiggelen, Nat. Phys. **4**, 945 (2008).
[4]G. Roati, C. D. Errico, L. Fallani, M. Fattori, C. Fort, M. Zaccanti, G. Modugno, M. Modugno, and M. Inguscio, Nature **453**, 895 (2008).
[5]D. S. Wiersma, P. Bartolini, A. Lagendijk, and R. Righini, Nature **390**, 671 (1997).
[6]T. Sperling, W. Buehrer, C. M. Aegerter, and G. Maret, Nat. Photonics **7**, 48 (2013).
[7]S. E. Skipetrov and I. M. Sokolov, Phys. Rev. Lett. **112**, 023905 (2014).
[8]S. Gottardo, R. Sapienza, P. D. García, A. Blanco, D. S. Wiersma, and C. López, Nat. Photonics **2**, 429 (2008).
[9]M. Florescu, S. Torquato, and P. J. Steinhardt, Proc. Natl. Acad. Sci. **106**, 20658 (2009).
[10]K. Vynck, M. Burresi, F. Riboli, and D. S. Wiersma, Nat. Mater. **11**, 1017 (2012).
[11]H. De Raedt, A. Lagendijk, and P. de Vries, Phys. Rev. Lett. **62**, 47 (1989).
[12]T. Schwartz, G. Bartal, S. Fishman, and M. Segev, Nature **446**, 52 (2007).
[13]S. Karbasi, C. R. Mirr, P. G. Yarandi, R. J. Frazier, K. W. Koch, and A. Mafi, Opt. Lett. **37**, 2304 (2012).
[14]S. Karbasi, T. Hawkins, J. Ballato, K. W. Koch, and A. Mafi, Opt. Mater. Express **2**, 1496 (2012).
[15]B. Abaie, E. Mobini, S. Karbasi, T. Hawkins, J. Ballato, and A. Mafi, Light: Sci. Appl. **6**, e17041 (2017).
[16]S. Karbasi, R. J. Frazier, K. W. Koch, T. Hawkins, J. Ballato, and A. Mafi, Nat. Commun. **5**, 3362 (2014).
[17]M. Leonetti, S. Karbasi, A. Mafi, and C. Conti, Phys. Rev. Lett. **112**, 193902 (2014).
[18]M. Leonetti, S. Karbasi, A. Mafi, and C. Conti, Appl. Phys. Lett. **105**, 171102 (2014).
[19]M. Leonetti, S. Karbasi, A. Mafi, E. DelRe, and C. Conti, Sci. Rep. **6**, 29918 (2016).
[20]A. Crespi, M. Bentivegna, I. Pitsios, D. Rusca, D. Poderini, G. Carvacho, V. D. Ambrosio, A. Cabello, F. Sciarrino, and R. Osellame, ACS Photonics **4**, 2807 (2017).
[21]S. Nolte, M. Will, J. Burghoff, and A. Tuennermann, Appl. Phys. A **77**, 109 (2003).
[22]R. R. Gattass and E. Mazur, Nat. Photonics **2**, 219 (2008).
[23]C. B. Schaffer, A. Brodeur, J. F. García, and E. Mazur, Opt. Lett. **26**, 93 (2001).
[24]R. Osellame, S. Taccheo, M. Marangoni, R. Ramponi, P. Laporta, D. Polli, S. De Silvestri, and G. Cerullo, J. Opt. Soc. Am. B **20**, 1559 (2003).
[25]L. Dominici, D. Colas, S. Donati, J. P. Restrepo Cuartas, M. De Giorgi, D. Ballarini, G. Guirales, J. C. López Carreño, A. Bramati, G. Gigli, E. del Valle, F. P. Laussy, and D. Sanvitto, Phys. Rev. Lett. **113**, 226401 (2014).
[26]S. M. Eaton, M. L. Ng, R. Osellame, and P. R. Herman, J. Non-Cryst. Solids **357**, 2387 (2011).
[27]V. Maselli, R. Osellame, G. Cerullo, R. Ramponi, P. Laporta, L. Magagnin, and P. L. Cavallotti, Appl. Phys. Lett. **88**, 191107 (2006).
[28]R. Osellame, V. Maselli, R. M. Vazquez, R. Ramponi, and G. Cerullo, Appl. Phys. Lett. **90**, 231118 (2007).
[29]A. Ródenas, M. Gu, G. Corrielli, P. Paiè, S. John, A. K. Kar, and R. Osellame, Nat. Photonics **13**, 105 (2019).
[30]S. Serajmohammadi and H. Alipour-Banaei, Front. Optoelectron. **6**, 346 (2013).
[31]G. Ruocco, B. Abaie, W. Schirmacher, A. Mafi, and M. Leonetti, Nat. Commun. **8**, 14571 (2017).
[32]L. Martin, G. Di Giuseppe, A. Perez-Leija, R. Keil, F. Dreisow, M. Heinrich, S. Nolte, A. Szameit, A. F. Abouraddy, D. N. Christodoulides *et al.*, Opt. Express **19**, 13636 (2011).
[33]L. Sapienza, H. Thyrrestrup, S. Stobbe, P. D. Garcia, S. Smolka, and P. Lodahl, Science **327**, 1352 (2010).
[34]W. Schirmacher, B. Abaie, A. Mafi, G. Ruocco, and M. Leonetti, Phys. Rev. Lett. **120**, 067401 (2018).
[35]P. A. Lee and T. Ramakrishnan, Rev. Mod. Phys. **57**, 287 (1985).
[36]A. Jesacher and M. J. Booth, Opt. Express **18**, 21090 (2010).